Available online at www.sciencedirect.com
ScienceDirect
Trans. Nonferrous Met. Soc. China 23(2013) 3033−3039
Transactions of Nonferrous Metals Society of China
www.tnmsc.cn

Determination of interfacial adhesive properties for polymeric film by blister test

Zi-han WANG[1,2], Zeng-sheng MA[1,2], Yi-chun ZHOU[1,2], Chun-sheng LU[3]

1. Key Laboratory of Low Dimensional Materials and Application Technology of Ministry of Education, Xiangtan University, Xiangtan 411105, China;
2. Faculty of Materials, Optoelectronics and Physics, Xiangtan University, Xiangtan 411105, China;
3. Department of Mechanical Engineering, Curtin University, Western Australia 6845, Australia

Received 17 October 2012; accepted 25 April 2013

Abstract: The interfacial adhesive properties of polypropylene/stainless steel were studied by the blister test. The polypropylene film with a squared free-standing window was pressured by oil from one side of film. The corresponding deformation field was observed by a digital speckle correlation method. The experimental results show that the squared film deforms and debonds from stainless steel with the increase of pressure. The debonding of the squared film in initiates from the center of edge and extends to the corner, and then the deformation of film evolves from square to circle shape. The interfacial adhesive energy of polypropylene/stainless steel is (22.60±1.55) J/m^2, which is in agreement with that measured by film with a circular window.

Key words: blister test; polymeric film; interfacial adhesive properties; debonding; whole-filed deformation

1 Introduction

The interfacial adhesion is a crucial factor to determine the performance of a coating or thin film on substrate [1−6]. A lot of methods have been proposed to characterize the interfacial adhesive properties of a coating/substrate system, such as cross-cut tape [7], peeling [8−10], nanoindentation [11−13], scratching [14−16] and blister tests [17−20]. In contrast to peeling and nanoindentation methods, the blister test is widely applied in the study of interfacial adhesive failure of various coatings [19,21−23]. As illustrated in Fig. 1(a), film firstly deflects outwards (i.e., the bulge test) under the uniform pressure p, forming a bulge with a constant diameter and an increasing altitude. When the pressure increases a small value of Δp, the film starts to debond from substrate with the debonding radius of Δa and the deflection of $\Delta\omega_0$ (i.e., the blister test) (see Fig. 1(b)).

DANNENBERG [24] initially proposed the blister test to measure the adhesion of thick organic coatings on metals. Later, WILLIAMS [25] introduced the pressurized circular blister test to measure the adhesive fracture energy of an elastomer film, and applied it to the debonding problem in engineering design. Based on the equation, LEE et al [19] extracted the adhesion energy between a silver electrode and pure barium titanate from experimental data. With these blister tests, the critical crack propagation energy of porous Ag/$BaTiO_3$ interface was measured and its average value is 2.5 J/m^2.

The deformation measurement in blister tests is essential for the determination of mechanical properties and the selection of materials. The digital speckle correlation method (DSCM) can be used to measure the whole-field deformation through the analysis of speckles on the specimen surface before and after deformation [26]. In comparison with traditional optical methods, DSCM has the advantages of high accuracy, simple optical arrangement, and without the requirement of vibration isolation [27,28]. Based on DSCM, ZHU et al [27] proposed an accurate 3D measurement system and its availability and reliability were validated by experiments. YAN et al [28] used DSCM to realize the orientation function of an optical mouse with a higher resolution.

In blister tests, the observed window of a free-standing film is circular and thus debonding is uniform along its edge [29,30]. CATLIN and WALKER

Foundation item: Projects (11102176, 11172258, 10828205) supported by the National Natural Science Foundation of China
Corresponding author: Zeng-sheng MA, Yi-chun ZHOU; Tel: +86-731-58293586; E-mail: zsma@xtu.edu.cn; zhouyc@xtu.edu.cn
DOI: 10.1016/S1003-6326(13)62830-7

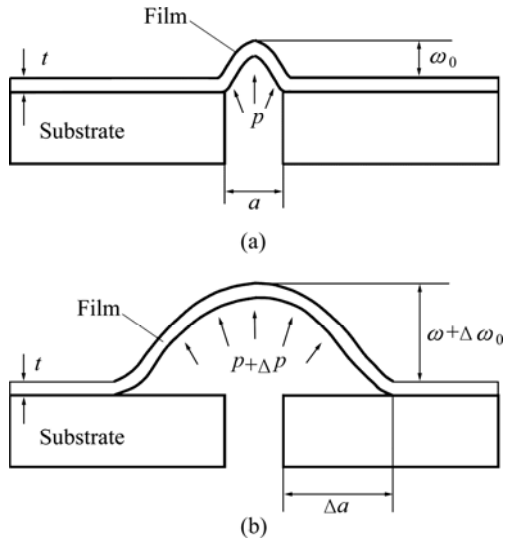

Fig. 1 Schematic of bulge test (a) and blister test (b)

[31] prepared the specimens by depositing gold films on sodium chloride crystal substrate blanks and drilling a small circle hole through the substrate with a water jet. KAENEL et al [32] fabricated the specimens by spark machining a hole in aluminum plates. In these traditional blister tests, the results such as elastic modulus are rather sensitive to the small variation of film dimensions. With the development of micromachining techniques, it is possible to precisely fabricate blister specimens. For example, the specimen dimensions can be controlled by standard lithography and anisotropic etching techniques [33]. Because of the anisotropic etching of Si substrate, however, the observed window of a free-standing film is squared or rectangled. Although the mechanical properties of various films (e.g., nitride, polymer, Inconel and metal films [33−36]) deposited on Si substrate, such as elastic modulus, residual stress, and Poisson ratio, have been measured, few studies are made to take the interfacial adhesion into considerations. In this work, the whole deformation field and debonding process by DSCM are measured. The interfacial adhesive energy of polypropylene/stainless steel with a squared free-standing film window is studied by the blister test. In addition, the stress field can be obtained from the whole deformation field.

2 DSCM principle

As illustrated in Fig. 2, the DSCM includes two parts: in-plane and out-of-plane displacement measurements. In Figs. 2(a) and (b), $P(x_P, y_P)$ and $Q(x_Q, y_Q)$ are the two points on the surface image of a specimen before deformation. After deformation, points P and Q move to P^* and Q^*, respectively. The in-plane strain components can be written as follows [37]:

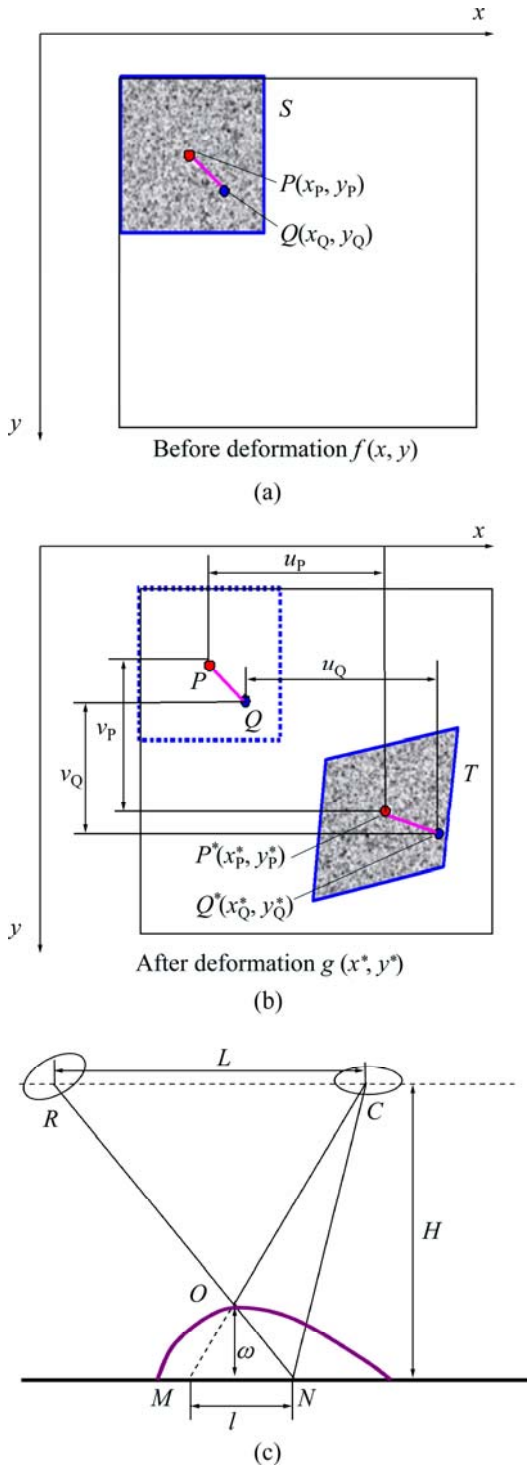

Fig. 2 Illustration of principle of DSCM: (a) In-plane displacements before deformation; (b) In-plane displacements after deformation; (c) Out-plane displacements

$$\begin{cases} \varepsilon_x = \dfrac{\partial u}{\partial x} + \dfrac{1}{2}\left[(\dfrac{\partial u}{\partial x})^2 + (\dfrac{\partial v}{\partial x})^2 \right] \\ \varepsilon_y = \dfrac{\partial v}{\partial x} + \dfrac{1}{2}\left[(\dfrac{\partial u}{\partial y})^2 + (\dfrac{\partial v}{\partial y})^2 \right] \\ \gamma_{xy} = \dfrac{1}{2}(\dfrac{\partial u}{\partial y} + \dfrac{\partial v}{\partial x}) + \dfrac{1}{2}\left[\dfrac{\partial u}{\partial x}\dfrac{\partial u}{\partial y} + \dfrac{\partial v}{\partial x}\dfrac{\partial v}{\partial y} \right] \end{cases} \quad (1)$$

Normally, to track the displacement of point P, a small squared subset S with $(2M+1)\times(2M+1)$ pixels around point P is chosen in the undeformed state. The position of the selected subset in the deformed image (named subset T) is obtained through searching the peak position of the distribution of correlation coefficient. Here, a typical correlation function is defined as [38]:

$$K=\sum_{i=-M}^{M}\sum_{j=-M}^{M}[f(x_i,y_j)-\bar{f}][g(x_i',y_j')-\bar{g}]/\left(\sqrt{\sum_{i=-M}^{M}\sum_{j=-M}^{M}[f(x_i,y_j)-\bar{f}]^2}\cdot\sqrt{\sum_{i=-M}^{M}\sum_{j=-M}^{M}[g(x_i',y_j')-\bar{g}]^2}\right) \quad (2)$$

where K is the correlation coefficient; $f(x_i, y_i)$ and $g(x_i, y_i)$ are the gray values of subsets S and T, respectively; $\bar{f}$ and $\bar{g}$ are their corresponding average gray values.

The principle of out-of-plane displacement measurement is shown in Fig. 2(c). Random speckles are projected on the specimen surface by the projector R. If the film is in the undeformed state, speckles are projected to point N and then reflected to point C (i.e., the center of charge coupled device (CCD) camera). After deformation, the speckles are projected to point O and reflected along the OC ray to the CCD camera. The point M is the prolongation end of the OC ray. According to the geometric relationship, the in-plane displacement l can be obtained as

$$l=\overline{MN}=L\omega/(H-\omega) \quad (3)$$

where H is the distance between the CCD camera and specimen and L is the distance between the projector and CCD camera. Due to $\omega \ll H$, Eq. (3) can be written as

$$\omega=(H/L)l \quad (4)$$

3 Experimental

A schematic of the blister test setup is shown in Fig. 3(a). The specimen was clamped onto the specimen holder that connects with the oil chamber. The pressure was applied by a stepper motor and measured by a pressure transducer. The deflection of the free-standing film was measured by DSCM. The white light was formed into speckle through the speckle fabrication and projected on the specimen surface via lens. The surface speckle images before and after deflection were recorded by a CCD camera.

A stainless steel disc was used as substrate with the diameter and thickness of 34 mm and 3 mm, respectively. A squared hole, with the length of 4 mm, was machined at the center of substrate. The surface of substrate was then roughened by using the abrasive paper. To avoid air bubbles between the film and substrate, specimens were carefully prepared by pressing polypropylene film with a thickness of about 50 μm on stainless steel, as shown in Fig. 3(b).

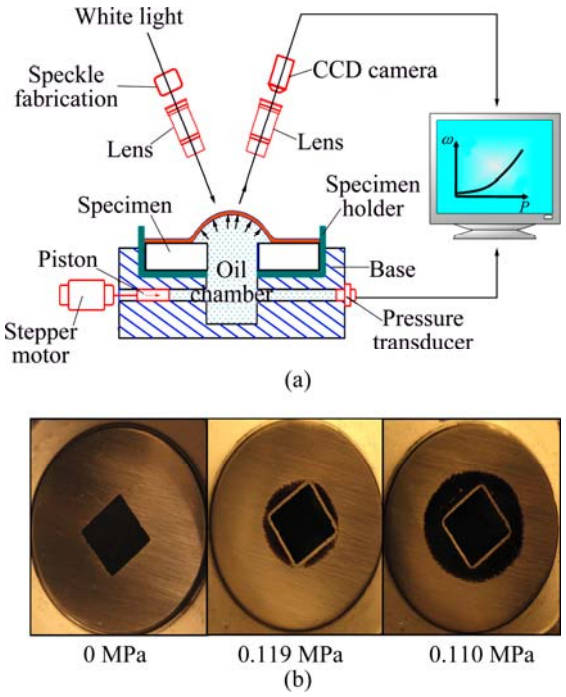

Fig. 3 Schematic of blister test setup (a) and photos of specimen at different pressures (b)

4 Results and discussion

4.1 Debonding process

The whole deformation fields of polypropylene film before and after debonding are given in Figs. 4 and 5, respectively. It is seen in Fig. 4 that the film stretches upward under a uniform pressure and the contour profile of deformation is squared. As shown in Fig. 5(a), the deflection of polypropylene film increases with increasing pressure. The debonding initiates from the centers of four edges and towards their corners (see Fig. 5(b)).

As shown in Fig. 6(a), at the pressures of 0.024 MPa and 0.076 MPa, the deflection of polypropylene film slowly increases. Beyond the critical pressure of 0.119 MPa, the squared film debonds from the centers of four sides (see insert in Fig. 6(a)). The pressures applied to polypropylene film decrease to 0.110 MPa and 0.100 MPa with the increase of cracking and deflection. The debonding process is clearly seen from the photo of specimen in Fig. 3(b). The debonding appears from the centers of edges at p=0.119 MPa. With the increase of the debonding zone, the pressure decreases to 0.110 MPa. The shape of debonded film becomes circular with further debonding. It is also seen in Fig. 6(b) that

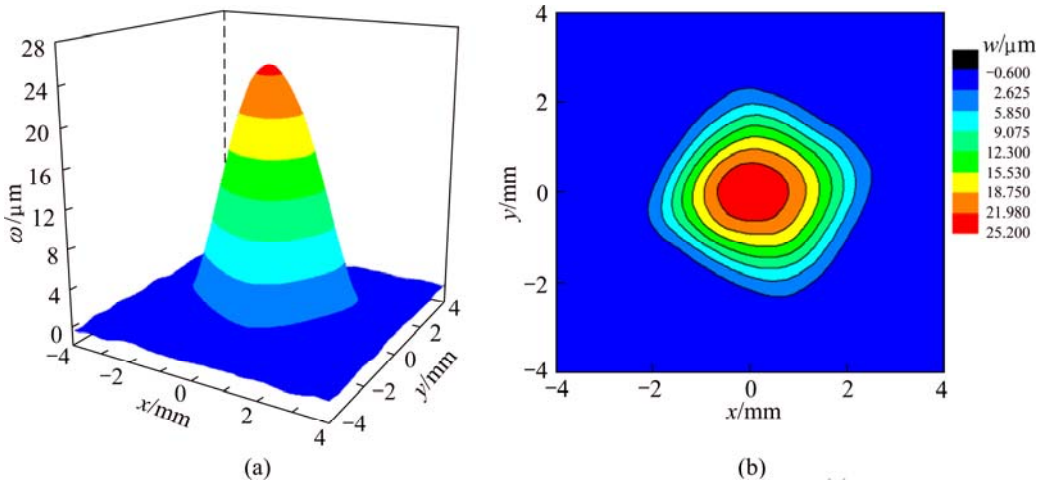

Fig. 4 Deformation field of polypropylene film before debonding at p=0.003 MPa: (a) 3D profile; (b) Contour map

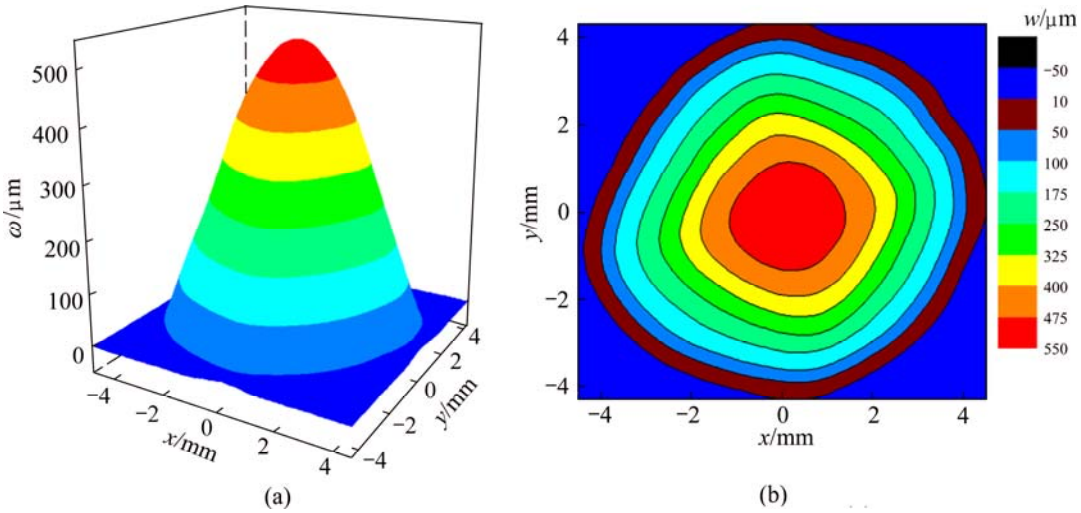

Fig. 5 Deformation field of polypropylene film after debonding at p=0.110 MPa: (a) 3D profile; (b) contour map

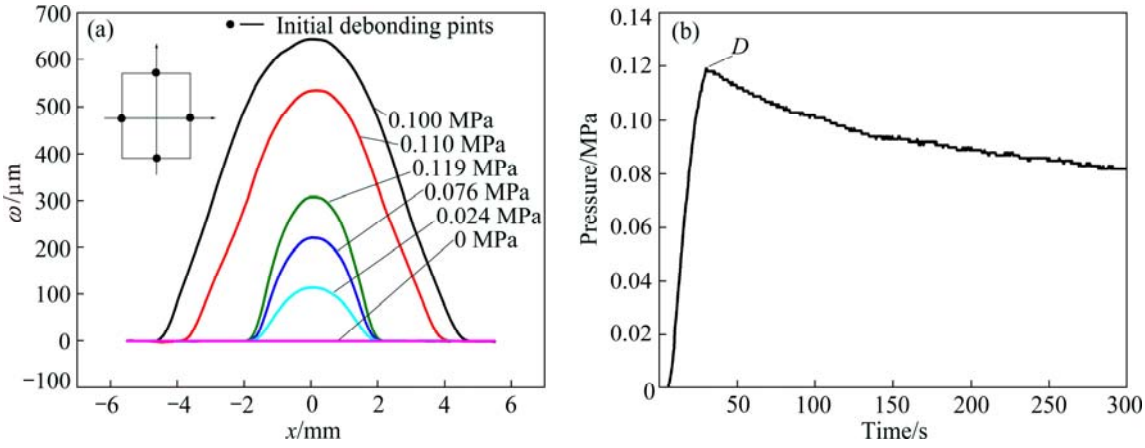

Fig. 6 Deflection in xz-plane at different pressures (a) and pressure—time curve (b) during debonding process

pressure monotonically increases at the beginning of the test. After the critical point D (p_c=0.119 MPa), there is debonding between film and substrate, which causes the decrease of pressure.

4.2 Stress fields

A free-standing squared film, with the thickness of t and the side of $2a$, is bonded to its substrate at the window edges. Let (u, v, ω) be the components of the

displacement parallel to the (x, y, z) directions (see Fig. 7(a)). Considering the clamped film edges, the boundary conditions are

$$\begin{cases} u=0, \omega=0, \dfrac{\partial\omega}{\partial x}=0 & \text{for } x=\pm a \\ v=0, \omega=0, \dfrac{\partial\omega}{\partial y}=0 & \text{for } y=\pm a \end{cases} \tag{5}$$

The displacement fields of a squared film with the side of $2a$ can be approximated by [39]

$$\begin{cases} u=c\sin\dfrac{\pi x}{a}\cos\dfrac{\pi y}{2a} \\ v=c\sin\dfrac{\pi y}{a}\cos\dfrac{\pi x}{2a} \\ \omega=\omega_0\cos\dfrac{\pi x}{2a}\cos\dfrac{\pi y}{2a} \end{cases} \tag{6}$$

where c and ω_0 are constants. If the deflection of a film is much larger than its thickness, the influence of bending can be ignored. Then, strains in the film are given by [33]

$$\begin{cases} \varepsilon_x=\dfrac{\partial u}{\partial x}+\dfrac{1}{2}\left(\dfrac{\partial\omega}{\partial x}\right)^2 \\ \varepsilon_y=\dfrac{\partial v}{\partial y}+\dfrac{1}{2}\left(\dfrac{\partial\omega}{\partial y}\right)^2 \\ \gamma_{xy}=\dfrac{\partial u}{\partial y}+\dfrac{\partial v}{\partial x}+\dfrac{\partial\omega}{\partial x}\dfrac{\partial\omega}{\partial y} \end{cases} \tag{7}$$

In the case of linear elasticity, the strain energy U can be expressed by

$$U=\frac{Et}{2(1-\nu^2)}\iint[\varepsilon_x^2+\varepsilon_y^2+2\nu\varepsilon_x\varepsilon_y+\frac{1}{2}(1-\nu)\gamma_{xy}^2]\mathrm{d}x\mathrm{d}y \tag{8}$$

where t, E, and ν are the thickness, elastic modulus and Poisson ratio of the film, respectively. According to the virtual displacement principle, we have

$$\begin{cases} \dfrac{\partial U}{\partial c}=0 \\ \dfrac{\partial U}{\partial\omega_0}\delta\omega_0=p\delta\omega_0\cos\dfrac{\pi x}{2a}\cos\dfrac{\pi y}{2a}\mathrm{d}x\mathrm{d}y \end{cases} \tag{9}$$

By solving Eq. (9), the parameters of c and ω_0 in Eq. (6) can be obtained as

$$\begin{cases} c=\dfrac{29.61\omega_0^2(-5+3\nu)}{a(24.83\nu-863.44)} \\ \omega_0=0.81\left(\dfrac{pa^4(862.63-24.74\nu)(\nu^2-1)}{Et(-1796.32\upsilon-2713.14+576\upsilon^2)}\right)^{1/3} \end{cases} \tag{10}$$

where p is the pressure applied to the film and a is the half side of the film. For the polypropylene film, υ=0.38 [40], Eq. (10) can be simplified as

$$\omega_0=0.777\left(\frac{pa^4}{Et}\right)^{1/3},\quad c=0.134\frac{\omega_0^2}{a} \tag{11}$$

The stresses in the film can be written as

$$\begin{cases} \sigma_x=\dfrac{E(1-\nu)}{(1+\nu)(1-2\nu)}\left(\varepsilon_x+\dfrac{\nu}{1-\nu}\varepsilon_y\right) \\ \sigma_y=\dfrac{E(1-\nu)}{(1+\nu)(1-2\nu)}\left(\varepsilon_y+\dfrac{\nu}{1-\nu}\varepsilon_x\right) \\ \sigma_z=\nu(\sigma_x+\sigma_y) \end{cases} \tag{12}$$

Figures 7(b) and (c) show respectively the stress fields of σ_x and σ_z in polypropylene film at the critical debonding pressure of 0.119 MPa and E=2 GPa [41]. In

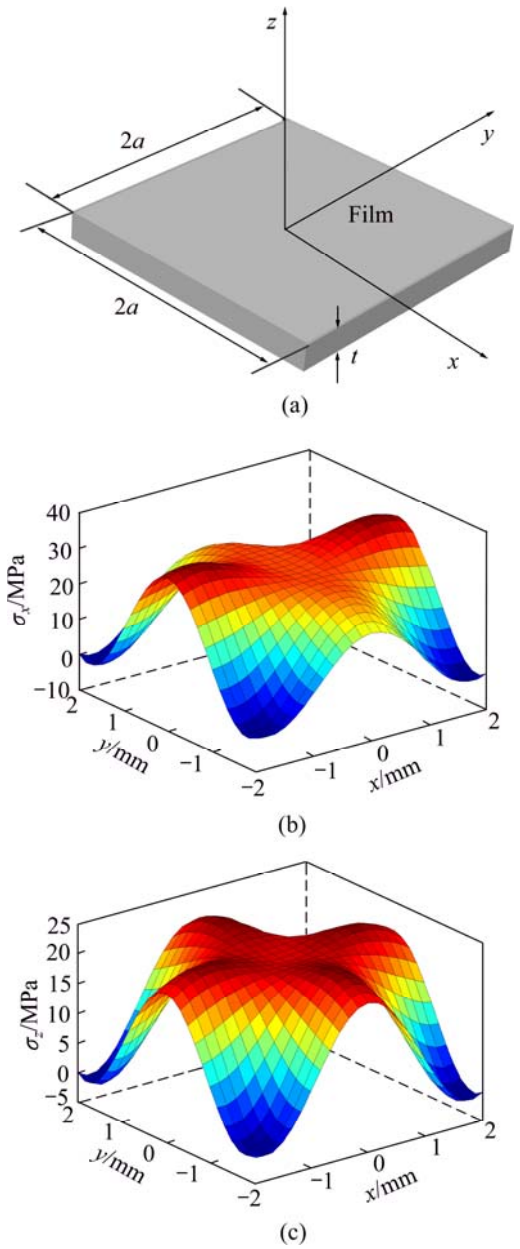

Fig. 7 Illustration of coordinate system (a) and stress fields of σ_x (b) and σ_z (c) in polypropylene film at p=0.119 MPa

Fig. 7(b), the maximum value of σ_x is distributed on both sides of x axis. It is seen in Fig. 7(c) that the maximum σ_z in film appears at the center of four edges and decreases to zero at the corners. According to the analysis of σ_z, the debonding of film occurs at the centers of four edges.

4.3 Interfacial adhesive energy

In the blister test, the film deforms under a uniform pressure. A part of the work done by the pressurizing oil is stored as the film's elastic strain energy, and the rest of the work is available to break the interfacial bonding. If there is no residual stress in the film, the interfacial adhesive energy G_c can be calculated by [42]

$$G_c = 1.25 p_c \omega_c \frac{\kappa_v}{\pi} \tag{13}$$

where p_c and ω_c are the critical debonding pressure and its corresponding deflection. The coefficient κ_v, which accounts for the shape of the film, is roughly 1.62 for circular windows and 1.94 for squared windows. Thus, the interfacial adhesive energy of a polypropylene film/stainless steel system is (22.60±1.55) J/m^2. To verify the result, the similar work is done on the circular film. The interfacial adhesive energy of a circular polypropylene film on stainless steel is (25.32±2.17) J/m^2, which is consistent with the result of a squared film.

5 Conclusions

The interfacial adhesive properties of a squared film on substrate were studied by the blister test. In contrast to the uniform debonding of a circular film, debonding appears from the centers of four edges of a squared film and then propagates to their corners. The experimental results are explained by the distribution of stresses in the z direction, where the largest values are at the centers of four edges. The interfacial adhesive energy of polypropylene/stainless steel is (22.60±1.55) J/m^2, which is in agreement with that obtained from a circular film.

References

[1] KENDALL K. Adhesion: Molecules and mechanics [J]. Science, 1994, 263(5154): 1720−1725.

[2] MANGIPUDI V S, TIRRELL M. Contact-mechanics-based studies of adhesion between polymers [J]. Rubber Chemistry and Technology, 1998, 71(3): 407−448.

[3] SUN X J, TAO J, GUO X Z. Bonding properties of interface in Fe/Al clad tube prepared by explosive welding [J]. Transactions of Nonferrous Metals Society of China, 2011, 21(10): 2175−2180.

[4] NAKANISHI R, SUEOKA K, SHIBA S, HINO M, MURAKAMI K, MURAOKA K. First principles calculation of stable structure and adhesive strength of plated Ni/Fe(100) or Cu/Fe(100) interfaces [J]. Transactions of Nonferrous Metals Society of China, 2009, 19(4): 988−991.

[5] SHEN B, SUN F H, ZHANG Z M, SHEN H S, GUO S S. Application of ultra-smooth composite diamond film coated WC−Co drawing dies under water-lubricating conditions [J]. Transactions of Nonferrous Metals Society of China, 2013, 23(1): 161−169.

[6] GAO X S, TIAN Z J, LIU Z D, SHEN L D. Interface characteristics of Al_2O_3−13%TiO_2 ceramic coatings prepared by laser cladding [J]. Transactions of Nonferrous Metals Society of China, 2012, 22(10): 2498−2503.

[7] TANG J L, ZUO Y, TANG Y M, XIONG J P. Composition and corrosion resistance of palladium film on 316L stainless steel by brush plating [J]. Transactions of Nonferrous Metals Society of China, 2012, 22(1): 97−103.

[8] WEI Y G, HUTCHINSON J W. Interface strength, work of adhesion and plasticity in the peel test [J]. International Journal of Fracture, 1998, 93(1): 315−333.

[9] EVANS A G, HUTCHINSON J W, WEI Y. Interface adhesion: Effects of plasticity and segregation [J]. Acta Materialia, 1999, 47(15−16): 4093−4113.

[10] WILLIAMS J A, KAUZLARICH J J. The influence of peel angle on the mechanics of peeling flexible adherends with arbitrary load-extension characteristics [J]. Tribology International, 2005, 38(11−12): 951−958.

[11] SANCHEZ J M, EL-MANSY S, SUN B, SCHERBAN T, FANG N, PANTUSO D, FORD W, ELIZALDE M R, MARTINEZ-ESNAOLA J M, MARTIN-MEIZOSO A, GIL-SEVILANO J, FUENTES M, MAIZ J. Cross-sectional nanoindentation: A new technique for thin film interfacial adhesion characterization [J]. Acta Materialia, 1999, 47(17): 4405−4413.

[12] ZHENG X J, ZHOU Y C. Investigation of an anisotropic plate model to evaluate the interface adhesion of thin film with cross-sectional nanoindentation method [J]. Composites Science and Technology, 2005, 65(9): 1382−1390.

[13] LI X F. Effects of an elastic substrate on the interfacial adhesion of thin films [J]. Surface and Coatings Technology, 2006, 200(16−17): 5003−5008.

[14] THOULESS M D. An analysis of spalling in the microscratch test [J]. Engineering Fracture Mechanics, 1998, 61(1): 75−81.

[15] LAUGIER M T. An energy approach to the adhesion of coatings using the scratch test [J]. Thin Solid Films, 1984, 117(4): 243−249.

[16] ZHOU L P, WANG M P, WANG R, LI Z, ZHU J J, PENG K, LI D Y, LI S L. Enhanced adhesion of Cu−W thin films by ion beam assisting bombardment implanting [J]. Transactions of Nonferrous Metals Society of China, 2008, 18(2): 372−377.

[17] VOLINSKY A A, MOODY N R, GERBERICH W W. Interfacial toughness measurements for thin films on substrates [J]. Acta Materialia, 2002, 50(3): 441−466.

[18] GENT A N, LEWANDOWSKI L H. Blow-off pressures for adhering layers [J]. Journal of Applied Polymer Science, 2003, 33(5): 1567−1577.

[19] LEE C Y, DUPEUX M, TUAN W H. Adhesion strength of Ag/$BaTiO_3$ interface [J]. Scripta Materialia, 2006, 54(3): 453-457.

[20] JIANG L M, ZHOU Y C, LIAO Y G, SUN C Q. A pressurized blister test model for the interface adhesion of dissimilar elastic-plastic materials [J]. Materials Science and Engineering A, 2008, 487(1−2): 228−234.

[21] TAHERI N, MOHAMMADI N, SHAHIDI N. An automatic instrument for measurement of interfacial adhesion of polymeric coatings [J]. Polymer Testing, 2000, 19(8): 959−966.

[22] XIAO L H, SU X P, WANG J H, ZHOU Y C. A novel blister test to evaluate the interface strength between nickel coating and low carbon steel substrate [J]. Materials Science and Engineering A, 2009, 501(1−2): 235−241.

[23] ZHOU Y C, HASHIDA T, JIAN C Y. Determination of interface fracture toughness in thermal barrier coating system by blister tests

[J]. Journal of Engineering Materials and Technology, 2003, 125(2): 176−182.

[24] DANNENBERG H. Measurement of adhesion by a blister method [J]. Journal of Applied Polymer Science, 1961, 5(14): 125−134.

[25] WILLIAMS M L. The continuum interpretation for fracture and adhesion [J]. Journal of Applied Polymer Science, 1969, 13(1): 29−40.

[26] CHU T C, RANSON W F, SUTTON M A, PETERS W H. Applications of digital-image-correlation techniques to experimental mechanics [J]. Experimental Mechanics, 1985, 25(3): 232−244.

[27] ZHU F P, LIU W W, SHI H J, HE X Y. Accurate 3D measurement system and calibration for speckle projection method [J]. Optics and Lasers in Engineering, 2010, 48(11): 1132−1139.

[28] YAN H T, WANG M, GE Y X, ZHOU J P. Used digital speckle correlation method to realize orientation function of optical mouse [J]. Optics Communications, 2008, 281(18): 4741−4743.

[29] SHIRANI A, LIECHTI K M. A calibrated frature process zone model for thin film blistering [J]. International Journal of Fracture, 1998, 93(1): 281−314.

[30] GUO S, WAN K T, DILLARD D A. A bending-to-stretching analysis of the blister test in the presence of tensile residual stress [J]. International Journal of Solids and Structures, 2005, 42(9−10): 2771−2784.

[31] CATLIN A, WALKER W P. Mechanical properties of thin single-crystal gold films [J]. Journal of Applied Physics, 1960, 31(12): 2135−2139.

[32] von KAENEL Y, GIACHETTO J C, STIEGLER J, DREZET J M, BLANK E. A new interpretation of bulge test measurements using numerical simulation [J]. Diamond and Related Materials, 1996, 5(6−8): 635−639.

[33] VLASSAK J J, NIX W D. A new bulge test technique for the determination of Young's modulus and Poisson's ratio of thin films [J]. Journal of Materials Research, 1992, 7(12): 3242−3249.

[34] HUANG C K, LOU W M, TSAI C J, WU T C, LIN H Y. Mechanical properties of polymer thin film measured by the bulge test [J]. Thin Solid Films, 2007, 515(18): 7222−7226.

[35] FLEURY G, MALHAIRE C, POPULAIRE C, VERDIER M, DEVOS A, CHARVET P L, POLIZZI J P. Mechanical cross-characterization of sputtered inconel thin films for MEMS applications [J]. Sensors and Actuators B, 2007, 126(1): 48−51.

[36] KALKMAN A J, VERBRUGGEN A H, JANSSEN G C A M. Young's modulus measurements and grain boundary sliding in free-standing thin metal films [J]. Applied Physics Letters, 2001, 78(18): 2673−2675.

[37] JIN Guan-chang. Computer aided optical measurement [M]. Beijing: Tsinghua University Press, 1997. (in Chinese)

[38] PAN B, WU D, XIA Y. High-temperature deformation field measurement by combining transient aerodynamic heating simulation system and reliability-guided digital image correlation [J]. Optics and Lasers in Engineering, 2010, 48(9): 841−848.

[39] TIMOSHENKO S, WOINOWSKY-KRIEGER S. Theory of plates and shells [M]. New York: McGraw-Hill, Inc, 1959.

[40] STARKE J U, MICHLER G H, GRELLMANN W, SEIDLER S, GAHLEITNER M, FIEBIG J, NEZBEDOVA E. Fracture toughness of polypropylene copolymers: Influence of interparticle distance and temperature [J]. Polymer, 1998, 39(1): 75−82.

[41] NIE H Y, WALZAK M J, MCINTYRE N S. Scratch resistance anisotropy in biaxially oriented polypropylene and poly(ethylene terephthalate) films [J]. Applied Surface Science, 2006, 253(4): 2320−2326.

[42] HOHLFELDER R J, LUO H, VLASSAK J J, CHIDSEY C E D, NIX W D. Measuring interfacial fracture toughness with the blister test [C]//BAKER S P, GAO J, GERBERICH W W, SUNDGREN J E. MRS Proceedings. San Francisco: Cambridge University Press, 1996: 115−120.

鼓包法表征聚合物薄膜的界面粘接性能

王子菡[1,2]，马增胜[1,2]，周益春[1,2]，卢春生[3]

1. 湘潭大学 低维材料及其应用技术教育部重点实验室，湘潭 411105；
2. 湘潭大学 材料与光电物理学院，湘潭 411105；
3. 科廷大学 机械工程系，西澳大利亚州 6845，澳大利亚

摘 要：采用鼓包法研究聚丙烯薄膜/不锈钢基底的粘接性能。基于数字散斑相关法，对自由窗口的聚丙烯薄膜受油压发生变形的全场形貌进行测量。实验结果表明：方形窗口薄膜的剥离最先从四边的中心开始，然后扩展到薄膜的 4 个尖角，变形形貌从方形最后变成圆形。聚丙烯薄膜/不锈钢基底的界面粘接能为(22.60±1.55) J/m^2，这个结果和圆形薄膜窗口测量的结果吻合得较好。

关键词：鼓包法；聚合物薄膜；界面粘接性能；脱粘；全场变形

(Edited by Hua YANG)